A Two-Level Wind and Buoyancy Driven Thermocline Model

PETER D. KILLWORTH*

Department of Applied Mathematics and Theoretical Physics, University of Cambridge, Cambridge, England

(Manuscript received 6 August 1984, in final form 30 April 1985)

ABSTRACT

A simple two-level model is designed to simulate the "thermocline equations," applicable for large-scale steady oceanic flow. The model serves two functions. First, it replaces problems with the interpretation of slablike dynamics (e.g., Luyten *et al.*, 1983) by using continuously horizontally varying buoyancy, but at the cost of reducing the vertical resolution drastically. The equations used are geostrophy (plus a small linear drag to close a Stommel-like western boundary layer), mass conservation, and buoyancy conservation with a small but necessary horizontal diffusion. (Inclusion of vertical diffusion has little effect.) The ocean is driven by an Ekman layer, whose functions are to provide a given surface input of mass (through Ekman pumping) and buoyancy (through a specified buoyancy in the Ekman layer), i.e., to maintain the same boundary conditions as in classical thermocline studies. Sidewall conditions are not well understood and are almost certainly overspecified in this formulation. Second, the model works toward the development of a simple numerical model which can permit rapid, cheap evaluation of the ocean circulation on climatic timescales.

The depth integrated flow is known from the Ekman pumping, so that the only unknown flow is the (single) baroclinic mode, which may be derived from the thermal wind equations as the density field is advected and diffused. The time taken to a steady solution is a few hundred years for a two-gyre basin of side 4000 km.

Despite the apparent simplicity of the model, the solution is fairly realistic and quite complicated. The solution involves convective adjustment in the northern (cool) part of the basin. The area occupied by convection increases with the amplitudes of both buoyancy forcing and Ekman pumping. There is a strong western boundary current, that separates farther south of its equivalent North Atlantic latitude, and flows toward the northeast corner of the basin where there is strong downwelling as the flow is returned in the lower level. The average of the level densities serves as an approximate streamfunction for the baroclinic flow that spins up initially like a long Rossby wave response of a linear ocean to wind forcing. Transfer from the southern to the northern gyre is produced by diffusion and ageostrophic effects in midocean, and not at the western boundary.

To examine the ventilation of the lower subtropical level of the ocean, trajectories were examined for water particles emitted from the downwelling Ekman layer. Those released in the southern half of the subtropics have quite complex tracks, with a tendency for anticyclonic circulation for several years followed by a cross-gyre movement to the subpolar gyre and circuitous routes back to the subtropics. The net result seems to be little direct ventilation. Particles released nearer the gyre boundary also show little tendency to direct lower ventilation. Adding random walks to the particle tracks to simulate the horizontal diffusivity shows that diffusion made little qualitative difference apart from an expected smearing out of the tracks.

1. Introduction

The ocean is driven primarily by processes occurring at its surface. Wind stress drives horizontal fluxes in the surface mixed layer and produces Ekman divergence at its base. Surface buoyancy fluxes (due to heating/cooling and evaporation/precipitation) yield varying densities in the upper layer of the ocean that drive motions through the resulting pressure imbalance.

Whereas motions on short timescales (days to months) are dominated by wind driving, those on longer time scales are produced by an intricate and highly nonlinear interaction between wind and buoyancy effects. It is this nonlinear aspect—induced by advection of buoyancy, if not momentum—that has inhibited understanding of ocean circulation on climatic time scales.

One solution has been to examine the steady-state response to surface forcing; this response is implicitly large-scale and excludes many of the direct effects of eddy motions. The period between the late 1950s and the early 1970s saw much work on the "thermocline equations," i.e., conservation of mass and buoyancy, together with the geostrophic and hydrostatic relations. These equations are mathematically quite curious and possess a variety of similarity solutions (Welander, 1971, discusses these in detail). They cannot, however, hold throughout an entire midlatitude basin, as no western boundary layer is permitted.

In the past few years, interest in the dynamics represented by these equations have reappeared because of the growing need to add to our understanding of the oceanic circulation by using information contained in

* Current affiliation: Hooke Institute for Atmospheric Research, Clarendon Laboratory, Oxford, England.

the buoyancy field. Inverse calculations (e.g., Schott and Stommel, 1978; Wunsch and Grant, 1982; or Killworth, 1983a) have used these dynamics as a basis for constructing best-fit solutions to flow fields from density observations. The active tracer, linearised potential vorticity is also conserved, and maps of potential vorticity on density surfaces have been constructed as an aid to understanding the constraints on the large-scale circulation (McDowell *et al.*, 1982).

In parallel with these developments has been a return to an examination of the solutions to the thermocline equations themselves. In a series of papers, beginning with Luyten *et al.* (1983), these authors and their coworkers have explored the dynamics of a layered ocean driven by a specified Ekman pumping and surface density field (or, to be precise, known latitudes where each layer outcrops at the surface). Using potential vorticity conservation within layers, they were able to show the existence of "shadow zones" containing water that was never ventilated at the surface.

In common with all layered models, there is a problem of interpretation of layer thickness in terms of stratification, especially since the extension to a continuous stratification is not obvious. Additionally, there are problems about boundary conditions at rigid walls (cf. Pedlosky, 1983a; Killworth, 1983b; Huang, 1984) generic to thermocline theory. Indeed, the mathematical character of the thermocline equations is still not understood (cf. Huang, 1984, for a discussion).

The inclusion of dissipative effects means that potential vorticity is no longer conserved. Rhines and Young (1982) showed that closed, nearly horizontal streamlines would wind up lines of potential vorticity and then homogenize it, via dissipation. They predicted large pools of near-uniform potential vorticity that were also indicated in the maps of McDowell *et al.* (1982). Recently, Pedlosky (1983b) has argued that even small regions of surface forcing can overcome the tendency to homogenization (in his case, by Ekman pumping, though perhaps potential vorticity creation by retreating mixed layers in spring may be an even more efficient mechanism). The large-scale numerical solutions of Cox and Bryan (1984) seem to support both views. They find ventilated zones of low potential vorticity created in convective areas, together with pool zones which are never in contact with surface forcing. Similar analytical findings are given by Pedlosky and Young (1983).

There is a need for more large-scale models which contain the thermocline physics, permit a continuously varying forcing, and yet permit rapid evaluation of the solution. One such model is the Hamburg climate model (Hasselmann, 1982) which has, at its core, continuously stratified thermocline physics. Numerical problems in that model forced high viscosities (10^4 m^2 s^{-1}); a possible explanation for these problems will be given here. Another approach by Davey (1983) produced a two-level ocean model by truncating the Bryan (1969) multilevel model in a manner similar to Killworth (1974). The model was forced thermally to give only a baroclinic flow, although wind driving could be added.

The model to be discussed here draws on Davey's work, while also possessing similarities with some of the models of Pedlosky and Young. It will allow surface forcing in the manner normally used for thermocline studies: the surface density and the Ekman pumping are both specified, and act as joint driving forces. A simple linear drag is included to permit a western boundary layer that allows a closed midlatitude double gyre solution with a flat bottom.

Section 2 describes the model and Section 3 shows the natural decomposition into barotropic and baroclinic modes. Section 4 discusses the method of numerical solutions and the solutions themselves are given in Section 5. Some elementary analysis is given in Section 6 and the trajectories of water particles are discussed in Section 7.

2. The model

To allow for continuously varying density gradients in the horizontal, we use a model with two levels in the vertical resembling a vertically truncated Bryan (1969) model. Level and layer models both have advantages and disadvantages for modeling purposes. The rationale for choosing a level model is twofold: it allows a more precise specification of boundary conditions relating to buoyancy forcing and a great deal is known about the properties of level models (Bryan, 1969). The horizontal motion and density field are assumed vertically uniform within each level. All quantities may vary in the horizontal and vertical velocities linear in depth exist between the levels. On top of the upper level a mixed layer of uniform depth is placed giving the configuration shown in Fig. 1. The only function of the mixed layer is to mimic the boundary conditions of the thermocline equations by requiring it to provide two conditions for the interior flow in the levels beneath.

The first of these is dynamical: the Ekman vertical velocity w_s is specified at the base of the mixed layer. The second is a thermodynamic condition: the density of the mixed layer ρ_s is specified. (The complicated interactions of heat and salt that yield the actual density, both in the mixed layer and in the fluid below, are subsumed by this simple model into a single density field.) Thus, the mixed layer density is not allowed to be altered by upwelling from the interior fluid; later models will allow a proper dynamically and thermodynamically interacting mixed layer. Both ρ_s and w_s vary only north–south for simplicity.

The dynamics of the two levels are assumed almost geostrophic. The concept is that, over the majority of the ocean, the dynamics should be exactly geostrophic but that sufficient extension to geostrophy is made in

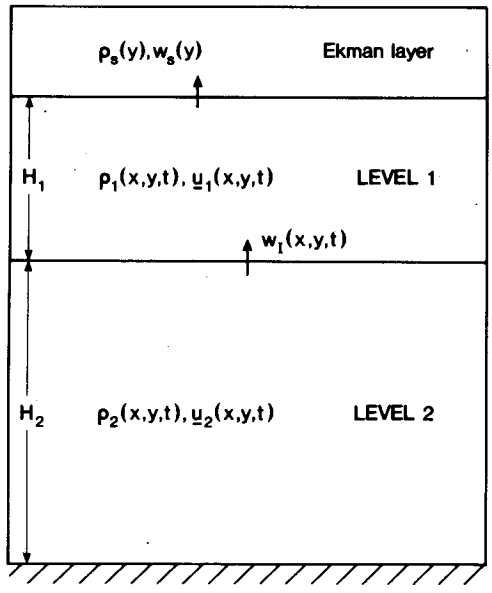

FIG. 1. The two-level model.

order to provide the simplest of western boundary currents to close the circulation. Accordingly, we allow for a linear drag term in the northward equation of motion, exactly paralleling the Stommel (1948) model of barotropic ocean circulation. There seems little point in using a higher-order closure scheme since the closure is only required near the western boundary current region and is hoped to be unimportant over the remainder of the flow. This may or may not be the case (cf. Young, 1984; Huang, 1984).

In a similar vein, we would like to require that density be a conserved quantity on a streamline that would again recreate the thermocline dynamics. Initial numerical experience showed this hope to be vain. Hence, a little lateral diffusion κ_T (10^3 m^2 s^{-1}) is included in the density equations. A vertical diffusion κ_v is included in the initial formulation, although its effects are small and will be ignored for most of this paper.

Mass continuity in the two levels then gives

$$w_I = H_1 \nabla \cdot \mathbf{u}_1 + w_s \tag{2.1}$$

$$w_I = -H_2 \nabla \cdot \mathbf{u}_2 \tag{2.2}$$

where w_I is the upwelling velocity at the base of level one and the divergence operator acts only horizontally. Density conservation in the two levels gives

$$\frac{\partial \rho_1}{\partial t} + \nabla \cdot (\mathbf{u}_1 \rho_1) + \frac{1}{H_1}(w_s \bar{\rho}_s - w_I \bar{\rho}_I) = \kappa_T \nabla^2 \rho_1 + \frac{\kappa_v}{H_1}\left[\frac{2(\rho_s - \rho_1)}{H_1} + \frac{4S}{H}\right] \tag{2.3}$$

$$\frac{\partial \rho_2}{\partial t} + \nabla \cdot (\mathbf{u}_2 \rho_2) + \frac{1}{H_2}(w_I \bar{\rho}_I) = \kappa_T \nabla^2 \rho_2 - \frac{4\kappa_v S}{H_2 H} \tag{2.4}$$

where

$$S = \tfrac{1}{2}(\rho_2 - \rho_1) \tag{2.5}$$

is a (nonnegative) measure of the vertical stratification and $\bar{\rho}_s$, $\bar{\rho}_I$ are as yet undefined densities at the interfaces between surface and upper level and upper and lower levels, respectively. The natural form of these values is suggested by conservation properties (Bryan, 1969):

$$\bar{\rho}_s = \tfrac{1}{2}(\rho_s + \rho_1); \quad \bar{\rho}_I = \tfrac{1}{2}(\rho_1 + \rho_2).$$

This formulation, however, has unpleasant side effects. Specifically, the lower level density can take values outside the range imposed by ρ_s in a steady state, which is physically meaningless. The effect occurs because centered vertical differencing produces a second, unphysical mode. A similar problem occurs in equatorial ocean models where the temperature in the highest level can exceed physical bounds.

Complicated multigrid methods exist to remove these effects, but this model only has two levels and cannot use them. We choose instead to abandon the analytic ease of centered differences in favor of more physical solutions and choose a one-sided difference scheme in the vertical, using upstream differences. We take

$$\left.\begin{aligned} \bar{\rho}_s &= \begin{cases} \rho_1, & w_s > 0 \\ \rho_s, & w_s < 0 \end{cases} \\ \bar{\rho}_I &= \begin{cases} \rho_2, & w_I > 0 \\ \rho_1, & w_I < 0 \end{cases} \end{aligned}\right\}. \tag{2.6}$$

One-sided differencing induces an artificial diffusion in the direction of differencing anyway, so that the imposed vertical diffusion has little effect and can be ignored. One of many alternative forms for (2.3), (2.4) is

$$\frac{\partial \rho_1}{\partial t} + \mathbf{u}_1 \cdot \nabla \rho_1 - \frac{2S w_I}{H_1}\bar{H}(w_I) + \frac{w_s}{H_1}(\rho_s - \rho_1)\bar{H}(-w_s) = \kappa_T \nabla^2 \rho_1 + O(\kappa_v) \tag{2.3'}$$

$$\frac{\partial \rho_2}{\partial t} + \mathbf{u}_2 \cdot \nabla \rho_2 + 2S\bar{H}(-w_I)\nabla \cdot \mathbf{u}_2 = \kappa_T \nabla^2 \rho_2 + O(\kappa_v) \tag{2.4'}$$

where $\bar{H}(x)$ is the Heaviside unit function and the vertical diffusion terms are as before and will be dropped henceforth. Note that answers using this scheme differ qualitatively from those using the Bryan scheme.

The momentum equations are exactly geostrophic north–south and almost so east–west:

$$-f v_1 = -\frac{1}{\rho_0}\frac{\partial p_1}{\partial x} \tag{2.7}$$

$$-f v_2 = -\frac{1}{\rho_0}\frac{\partial p_2}{\partial x} \tag{2.8}$$

$$fu_1 = -\frac{1}{\rho_0}\frac{\partial p_1}{\partial y} - \kappa v_1 \tag{2.9}$$

$$fu_2 = -\frac{1}{\rho_0}\frac{\partial p_2}{\partial y} - \kappa v_2, \tag{2.10}$$

where $f(y) \equiv f_0 + \beta y$ is the vertical component of the Coriolis force, p_i the pressure in level i, ρ_0 a reference density, and κ is a small linear drag to permit a Stommel-like western boundary layer. Here κ takes the value 4×10^{-6} s^{-1} numerically, corresponding to a decay time of about three days; the value is chosen to permit numerical resolution of the western boundary layer.

To close the equations, the hydrostatic condition must be added. Of the many forms possible, we follow Davey (1983) and take

$$p_2 - p_1 = \frac{1}{2} g(H_1 + H_2)\theta \tag{2.11}$$

where

$$\theta = \frac{1}{2}(\rho_1 + \rho_2). \tag{2.12}$$

Steady state solutions of (2.1)–(2.12) are to be found subject to given $w_s(y)$, $\rho_s(y)$. There are also boundary conditions to be satisfied. We take the basin to lie between $x = 0$ and $x = L$, $y = 0$ and $y = M$, and require

$$u_1 = u_2 = 0, \quad x = 0, L \tag{2.13}$$

$$v_1 = v_2 = 0, \quad y = 0, M. \tag{2.14}$$

Additionally, because of the diffusive terms, we shall require

$$\mathbf{n}\cdot\nabla\rho_1 = \mathbf{n}\cdot\nabla\rho_2 = 0, \quad x = 0, L; \quad y = 0, M \tag{2.15}$$

where $\mathbf{n}$ is an outward normal to the boundary.

It should be stressed that the mathematically correct boundary conditions for (2.1)–(2.12) are unknown (cf. the discussion by Huang, 1984). Certainly (2.13) to (2.15) overspecify the linear diffusive planetary wave problem, for example. Various boundary conditions have been tried numerically; at the coarse resolution used, little difference was observed between conditions. (I hope to discuss boundary conditions more fully in a later paper.)

Statically unstable solutions may occur, either those for which $S < 0$ ($\rho_1 > \rho_2$) or those for which $\rho_s > \rho_1$. In the former case, S is reset to zero and ρ_1 and ρ_2 are replaced by their depth-weighted average. In the latter case, the surface Ekman layer is assumed a reservoir with an infinite supply of ρ_s, and so ρ_1 (and if necessary ρ_2) is replaced by ρ_s.

3. Barotropic and baroclinic modes

We may resolve the velocity field $\mathbf{u}_1$, $\mathbf{u}_2$ into barotropic and baroclinic modes. Taking H_1 times (2.7) + H_2 times (2.8), and H_1 times (2.9) + H_2 times (2.10) gives

$$-fHV = -\frac{1}{\rho_0}P_x \tag{3.1}$$

$$fHU = -\frac{1}{\rho_0}P_y - \kappa HV \tag{3.2}$$

where

$$H = H_1 + H_2 \tag{3.3}$$

is the total depth,

$$H\mathbf{U} = H_1\mathbf{u}_1 + H_2\mathbf{u}_2 \tag{3.4}$$

is the barotropic (i.e., depth-independent) flow, and $P = H_1p_1 + H_2p_2$ is the depth integrated pressure. Eliminating the pressure gives

$$f\nabla\cdot\mathbf{U} + \beta V = -\kappa V_x. \tag{3.5}$$

Subtraction of (2.2) from (2.1) gives

$$\nabla\cdot\mathbf{U} = -\frac{w_s}{H} \tag{3.6}$$

(which is divergent because the Ekman layer flux is not included) so that

$$\kappa V_x + \beta V = \frac{fw_s(y)}{H} \tag{3.7}$$

represents the Sverdrup-Stommel solution for barotropic flow. Provided that $\kappa(\beta L)^{-1} \ll 1$, the solution of (3.7) is

$$V = \frac{fw_s}{\beta H} + Q(y)e^{-\beta x/\kappa} \tag{3.8}$$

for some $Q(y)$ that assumes $w_s(0) = w_s(M) = 0$ to avoid boundary layers at north and south walls. Then, (3.6) and (2.13) imply

$$U = -\frac{(x-L)}{H}\left(2w_s + \frac{f}{\beta}w_{sy}\right) + \frac{\kappa Q_y}{\beta}e^{-\beta x/\kappa} \tag{3.9}$$

where $Q(y)$ is now given by the requirement that U vanish on $x = 0$, i.e.,

$$Q = -\frac{\beta L}{\kappa H}\left(\int_0^y w_s dy + \frac{f}{\beta}w_s\right). \tag{3.10}$$

Thus, the vanishing of V on $y = M$ implies $Q(M) = 0$, so that consistency requires

$$\int_0^M w_s dy = 0 \tag{3.11}$$

i.e., no net up- or downwelling into the interior fluid. The width $\kappa\beta^{-1}$ of the boundary layer is 200 km, deliberately rather wide, and is just resolved numerically.

Thus, the barotropic flow is unaffected by density gradients and is known from the Ekman pumping condition. However, the baroclinic flow

$$\hat{\mathbf{u}} = \mathbf{u}_1 - \mathbf{u}_2 \tag{3.12}$$

will be driven almost entirely by the density field. Subtracting (2.8) from (2.7), and (2.10) from (2.9), and then using (2.11), gives the "thermal wind equations"

$$-f\hat{v} = \frac{gH}{2\rho_0}\theta_x \tag{3.13}$$

$$f\hat{u} = \frac{gH}{2\rho_0}\theta_y - \kappa\hat{v} \tag{3.14}$$

so that θ, defined by (2.11), serves as an approximate streamfunction for $f\hat{\mathbf{u}}$. Thus, $\hat{\mathbf{u}}\cdot\nabla\theta$ is small, by (3.13), (3.14), and we note for later use that

$$\nabla\cdot\mathbf{u} = \frac{gH}{2\rho_0 f^2}(\beta\theta_x + \kappa\theta_{xx}). \tag{3.15}$$

4. Method of numerical solution

Numerical solutions use a 20×20 C-grid discretization shown in Fig. 2 that has the advantage of placing the velocities normal to a wall exactly on that wall. Steady solution to the system of equations in Section 2 is achieved by time-stepping, as follows. First, U and V are computed from (3.8)–(3.10). [More properly, they are defined to satisfy the discretized form of (3.6) exactly]. Then ρ_1 and ρ_2 are set to some uniform initial values. At each time step, $\hat{v}$ is deduced from (3.13), and then $\hat{u}$ from (3.14), using centered and averaged differences. The values of normal velocity on the boundaries are set to zero identically. Then, $\mathbf{u}_1$, $\mathbf{u}_2$ are calculated from the definitions of $\mathbf{U}$ and $\hat{\mathbf{u}}$. These are used to drive the time-stepping of ρ_1 and ρ_2 in (2.3) and (2.4) using leapfrog time steps and time-lagged diffusive terms in the normal way. The new values of ρ_1, ρ_2 are used to update $\hat{u}$, $\hat{v}$ and the time-stepping proceeds.

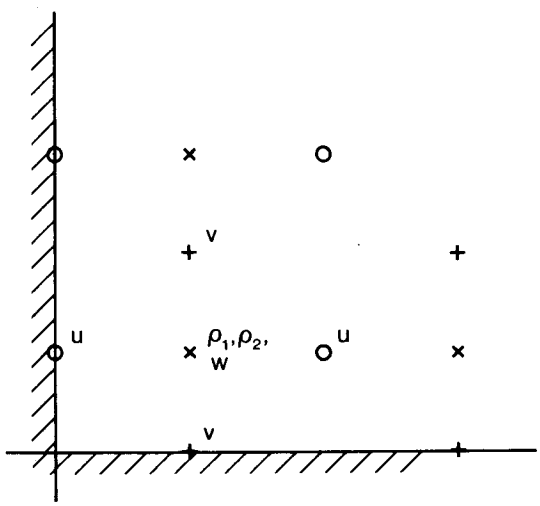

FIG. 2. The discretisation scheme used for numerical computation.

Various restrictions on the time step must be observed. The apparent virtue of the thermocline equations with a known barotropic field is that all motions more rapid than long internal Rossby waves have been filtered out of the dynamics, so that CFL criteria would allow a time step of the order of a month. Indeed, the Hamburg model (Hasselmann, 1982) uses this fact explicitly. Thus, the only obvious restrictions are for drag and diffusive terms, which are small and have little effect on the time step.

On running the model, however, a rapidly growing instability near the boundaries was observed. Experimentation showed this to be a linear instability associated with the condition of no normal flow at boundaries. In the Appendix it is shown that the change over one grid point between geostrophic flow and a rigid wall induces a numerical rapid tangential advection of density near the boundaries. The strength of the advection varies inversely with the grid spacing. For typical grid spacings of 200 km, the CFL condition requires a time step of the order of a day for stability. The effect is not unique to two-level simulations or one-sided differencing, and will occur in multilevel models. Since the restriction on time step is quadratic in both grid spacing and internal wave speed, the Hamburg model (Hasselmann, 1982) with its 5° spacing can apparently just manage a time step of a month; the need for the large viscosity may thus be to damp out marginally growing instabilities.

The results settle to an approximate steady state after several centuries, and results are quoted for 400 or more years of integration. The parameters used numerically are:

$$\Delta x = \Delta y = 200 \text{ km} \quad (L = M = 4000 \text{ km})$$
$$f = 10^{-4}\ \text{s}^{-1}, \qquad \beta = 2\times 10^{-11}\ \text{m}^{-1}\ \text{s}^{-1}.$$
$$H_1 = 400 \text{ m}, \qquad H_2 = 4000 \text{ m}$$
$$\kappa = 4\times 10^{-6}\ \text{s}^{-1}, \qquad \kappa_T = 10^3\ \text{m}^2\ \text{s}^{-1}$$

so that the spin-up time is approximately the diffusive time $L^2\kappa_T^{-1}$, as would be expected.

5. Numerical results

Two experiments will be reported; both used surface densities and Ekman suctions of the form

$$\rho_s(y) = -\rho_{so}\cos\pi y/M \tag{5.1}$$

$$w_s(y) = -w_{so}\sin 2\pi y/M \tag{5.2}$$

which are shown in Fig. 3. The value of ρ_{so} was always taken as 2×10^{-3} gm cm^{-3}; the value for w_{so} varied between experiments. The divergent barotropic field given by (3.8) and (3.9) is shown in Fig. 4 for $w_{so} = 10^{-4}$ cm s^{-1}; even in the western boundary layer barotropic velocities only reach a little over 1 cm s^{-1}.

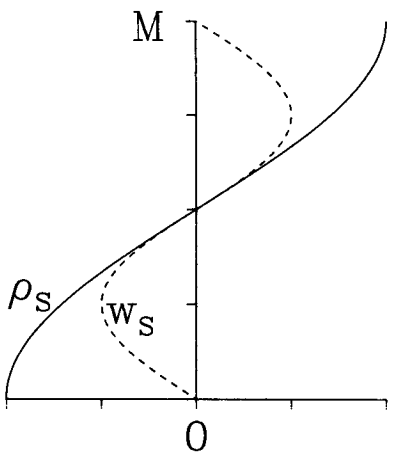

FIG. 3. The Ekman layer forcing and density, as functions of northward distance y.

a. Experiment 1: $w_{so} = 10^{-4}$ cm s^{-1}, ρ_1, ρ_2 = 1, 2 $\times 10^{-3}$ gm cm^{-3} initially

This experiment is taken as the standard case for the rest of the paper. The first five years of integration (Fig. 5) are dominated by the westward passage of a long Rossby wave, clearly visible in the southern half of the basin. A single gyre exists in the ρ_1, θ, and S fields at this time, but the ρ_2 field is largely unaffected save in the region of strong downwelling in the northeast corner of the basin. The variation in ρ_1 or θ is already some 60% of that for the final steady state. Overturning between mixed layer and level 1 is visible over much of the northern basin. The baroclinic velocity field is of order 10 cm s^{-1}, even away from the western boundary current.

The final steady state is shown in Fig. 6. The ρ_1 field (Fig. 6a) shows a large patch of light (i.e., warm) water in the south, but not skewed to the southwest as in the Atlantic or Pacific. Since the imposed ρ_s has a minimum of -2×10^{-3} gm cm^{-3}, but the most buoyant water has ρ_1 only just positive, there is effectively a strong pycnocline in the southern basin between ρ_s and ρ_1. Proceeding northward, there is a concentration of isopycnals in the western half of the basin that fans out and moves northeast to the eastern boundary. This feature is familiar from mean oceanographic data (cf. Levitus, 1982; or Esbensen and Kushnir, 1981). The corresponding current leaves the western boundary rather south of the latitude of zero wind stress curl. This is not the case for the Gulf Stream, however. The observed anomalous warming of the Northeast Atlantic by this current is reproduced here. The accompanying downwelling is rather less physical unless it is interpreted as the Greenland Sea sinking, as was suggested by Worthington (1970) as an alternative source of warm water for western Europe.

Farther north is a wide region of overturning from the Ekman layer to level 1. The region is narrowest in the northwest and widest in the northeast. There is also deep convection (level 1 to level 2) in the north, most clearly seen in the S field below. There are three main regions: the northwest corner, the northeast corner, and a narrow east–west oriented section touching the western boundary a little north of the gyre boundary. Both of the Robinson *et al.* (1979) and Levitus (1982) atlases show an increase eastward in depth of winter convection at 50–60°N in the Atlantic, which is perhaps the best field for comparison. Likewise, the northwestern convective region could be interpreted as the model version of the spasmodic deep convection in the Labrador Sea. Finally, there is some evidence in Levitus' (1982) atlas for denser water north of the Gulf Stream, and the area of deep convection here in the model could perhaps be interpreted as 18° water.

Figure 6b shows the lower level density. This is fairly zonal, and mainly increases northwards except for a reversal of gradient towards the northeast. Agreement with Levitus' (1982) maps of temperature at 1500–2000 m is striking, although the warm tongue in his maps is more properly a product of Mediterranean outflow.

Figure 6c shows the upper level velocity field. A pronounced anticyclonic surface gyre is evident in the subtropics, with a broad western boundary current that transports about 24 $\times$ 10^6 m^3 s^{-1} northwards at its

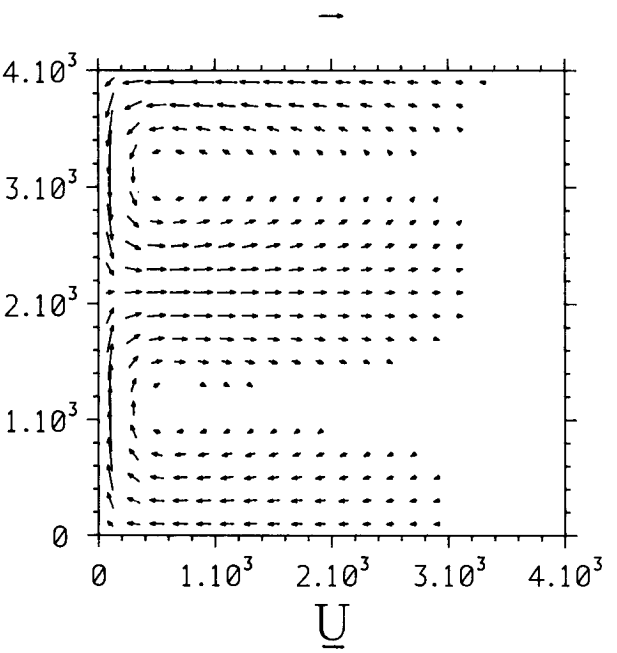

FIG. 4. The barotropic velocity field for $w_{so} = 10^{-4}$ cm s^{-1}. Arrow above the grid has length 1 cm s^{-1}. Arrow centers are placed on grid points; Distances are in km; Arrows shorter than arrowhead (i.e., shorter than 0.2 cm s^{-1}) not drawn.

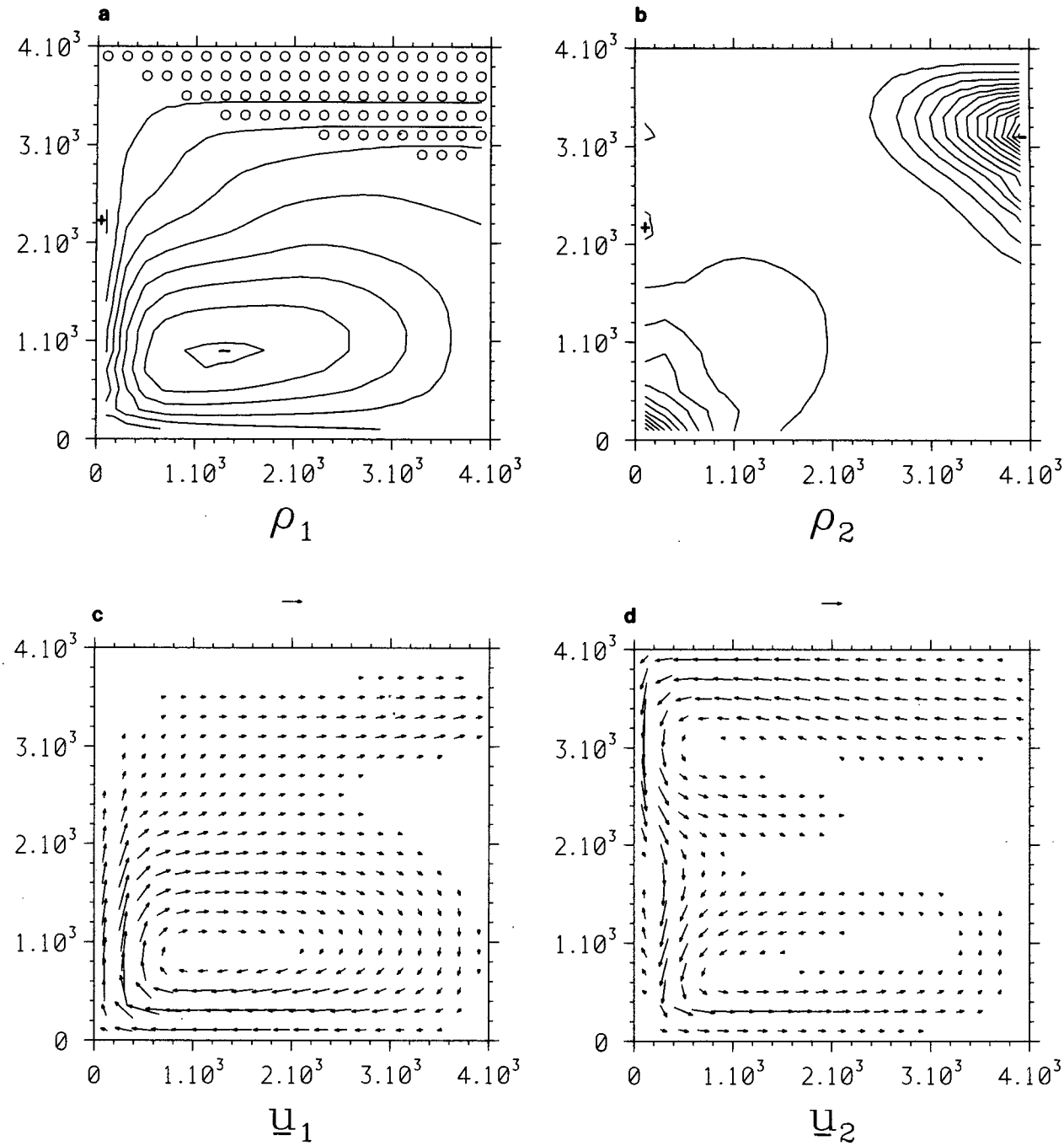

FIG. 5. The unsteady solution for case (a), after five years of forcing: (a) ρ_1, contour interval (c.i.) 2×10^{-4} g cm^{-3}, min 2.8×10^{-4}, max 2×10^{-3} g cm^{-3}; (b) ρ_2, c.i. 2×10^{-5} g cm^{-3}, min. 1.7×10^{-3}, max. 2×10^{-3} g cm^{-3}; (c) u_1, (arrow at top is 10 cm s^{-1}); (d) u_2, (arrow at top is 1 cm s^{-1}); (e) θ, c.i. 10^{-4} g cm^{-3}, min. 1.1×10^{-3}, max. 2×10^{-3}; (f) S, c.i. 10^{-4} g cm^{-3}, max. 8.3×10^{-4} g cm^{-3}. A plus sign shows the maximum and a minus sign shows the minimum of the contours. Circles show the area of convection between Ekman layer and level 1; squares the area of deep convection between levels 1 and 2.

maximum. The current leaves the coast as a broad jet and flows northeast across the basin carrying around 35×10^6 m^3 s^{-1} in the upper level. The picture resembles Leetmaa and Bunker's (1978, Fig. 4) dynamic topography map quite well, although topographic features clearly restrict the available paths for the Gulf Stream Extension. The model current turns north about halfway across the basin (again, similar to the

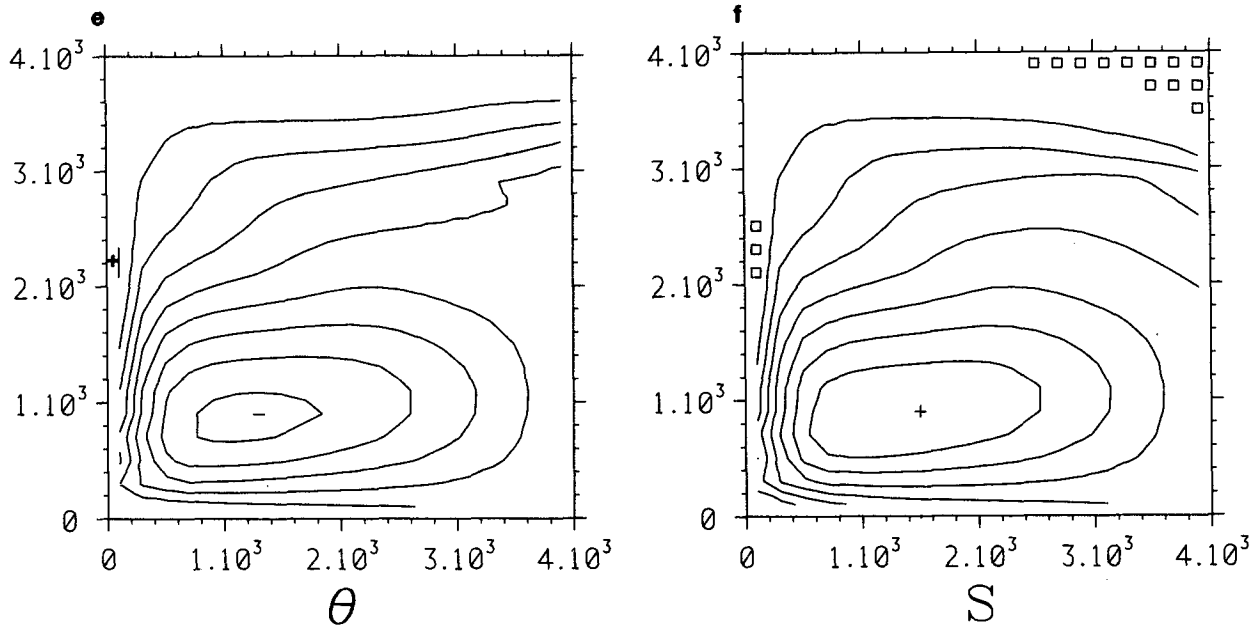

FIG. 5. (*Continued*)

Leetmaa and Bunker map) and then impinges on the coast to sink.

The upper layer flow resembles Huang's (1984) supercritical two layer solution. There, too, the western boundary layer leaves the coast and moves northeast into a weak subpolar gyre. However, it is returned in his model by a northern boundary current, whereas the overturning in this study prevents that.

The flow is returned (Fig. 6d) in the lower level (note the change of scale) in two branches. One is essentially baroclinic and follows the same path as $\mathbf{u}_1$ but with opposite sign; the other flows across the northern boundary and returns as a deep western boundary current (the model Labrador outflow) with a transport of 23×10^6 m^3 s^{-1}. Note that the subtropical deep western boundary current is northward and in the same direction as the upper level flow. There is an anticyclonic gyre in the northwestern subtropics, again, similar to Huang (1984), although produced in his model by interfacial friction.

Figure 6e shows the θ field, an approximate streamfunction for $f\hat{\mathbf{u}}$. The subtropical gyre is pronounced, and there is a tendency for long-shore gradients of θ to vanish at all but the western boundary as (3.13) and (3.14) suggest; the overturning in the north counters this effect. Figure 6f shows the stratification S, again reflecting the strong subtropical gyre. It is tempting to examine Rhines and Young's (1982) ideas on potential vorticity homogenisation using this map. However, no straightforward equation for fS, a measure of potential vorticity, can be written down for this system. The fractional change of fS is 68% across the basin, measured in terms of the maximum values of f and S, so there is some tendency toward uniformity of potential vorticity. More levels would be required to test out the hypothesis properly, however.

Figure 6g shows the interface vertical velocity w_I. Two very strong areas occur of upwelling at the western boundary near the zero wind stress curl latitude, and downwelling in the northeast corner. With this contour interval the remainder of the field is fairly featureless, with upwelling in the eastern basin and downwelling in the west, although most of the northern basin is upwelling. This suggests (see Section 7) that direct ventilation of the deep eastern subtropical gyre will be difficult.

b. Experiment 2: $w_{so} = 10^{-5}$ cm s^{-1}

Although the forcing and barotropic flow are weaker by a factor of 10 from experiment 1, the spinup time remains of the same order because diffusion effects become more important. Figure 7 shows the solution. The variation in ρ_1, ρ_2, θ, and S is smaller than the case $w_{so} = 10^{-4}$ cm s^{-1}, but not by a factor of 10. As we shall see, this is because density variations scale on $(w_{so})^{1/2}$. Although the flow is weaker, the solution remains qualitatively similar to case (a), with a single anticyclonic subtropical gyre and a (now diffuse) North Atlantic current; the area of overturning is much smaller than in case (a).

A further reduction of w_{so} to 10^{-6} cm s^{-1} again remains qualitatively similar and is not shown here. The overturning region shrinks to a single line of gridpoints

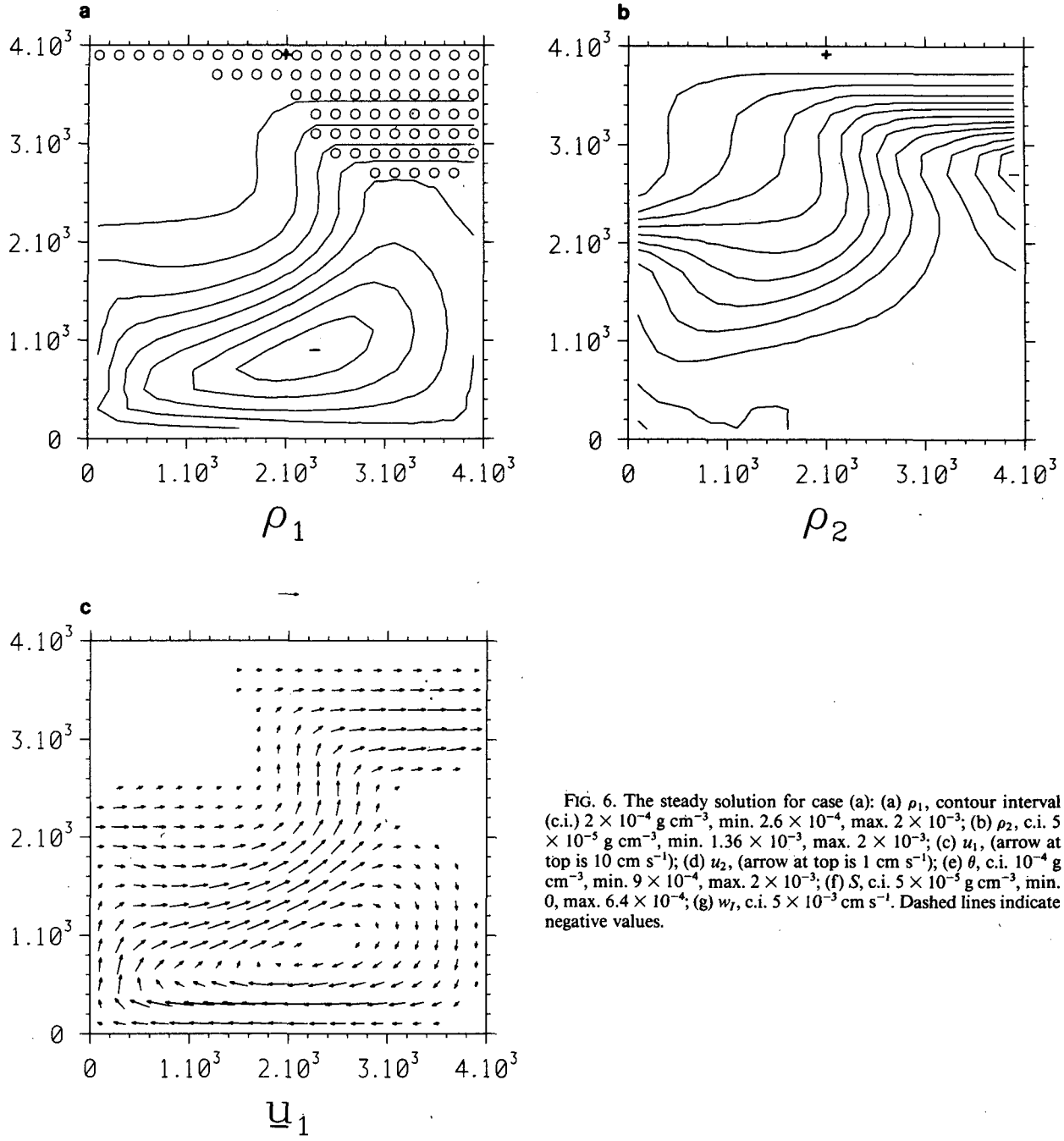

FIG. 6. The steady solution for case (a): (a) ρ_1, contour interval (c.i.) 2×10^{-4} g cm^{-3}, min. 2.6×10^{-4}, max. 2×10^{-3}; (b) ρ_2, c.i. 5×10^{-5} g cm^{-3}, min. 1.36×10^{-3}, max. 2×10^{-3}; (c) u_1, (arrow at top is 10 cm s^{-1}); (d) u_2, (arrow at top is 1 cm s^{-1}); (e) θ, c.i. 10^{-4} g cm^{-3}, min. 9×10^{-4}, max. 2×10^{-3}; (f) S, c.i. 5×10^{-5} g cm^{-3}, min. 0, max. 6.4×10^{-4}; (g) w_I, c.i. 5×10^{-3} cm s^{-1}. Dashed lines indicate negative values.

at the north, which is in agreement with the theory of the next section.

6. Analytical theory

The solutions in Section 5 show many interesting features. However, the problem remains complicated even after the simplifications made, and only simple arguments can be made to explain some of the observed features.

a. Convection

We first show that deep convection must occur in the steady state. Two proofs are useful, the first specific to the forcing used here, and the second quite general. Taking H_1 times (2.3) plus H_2 times (2.4) gives, for a steady flow,

$$\nabla \cdot (H_1 \mathbf{u}_1 \rho_1 + H_2 \mathbf{u}_2 \rho_2) = -w_s \tilde{\rho}_s + \kappa_T \nabla^2 (H_1 \rho_1 + H_2 \rho_2) + \phi \qquad (6.1)$$

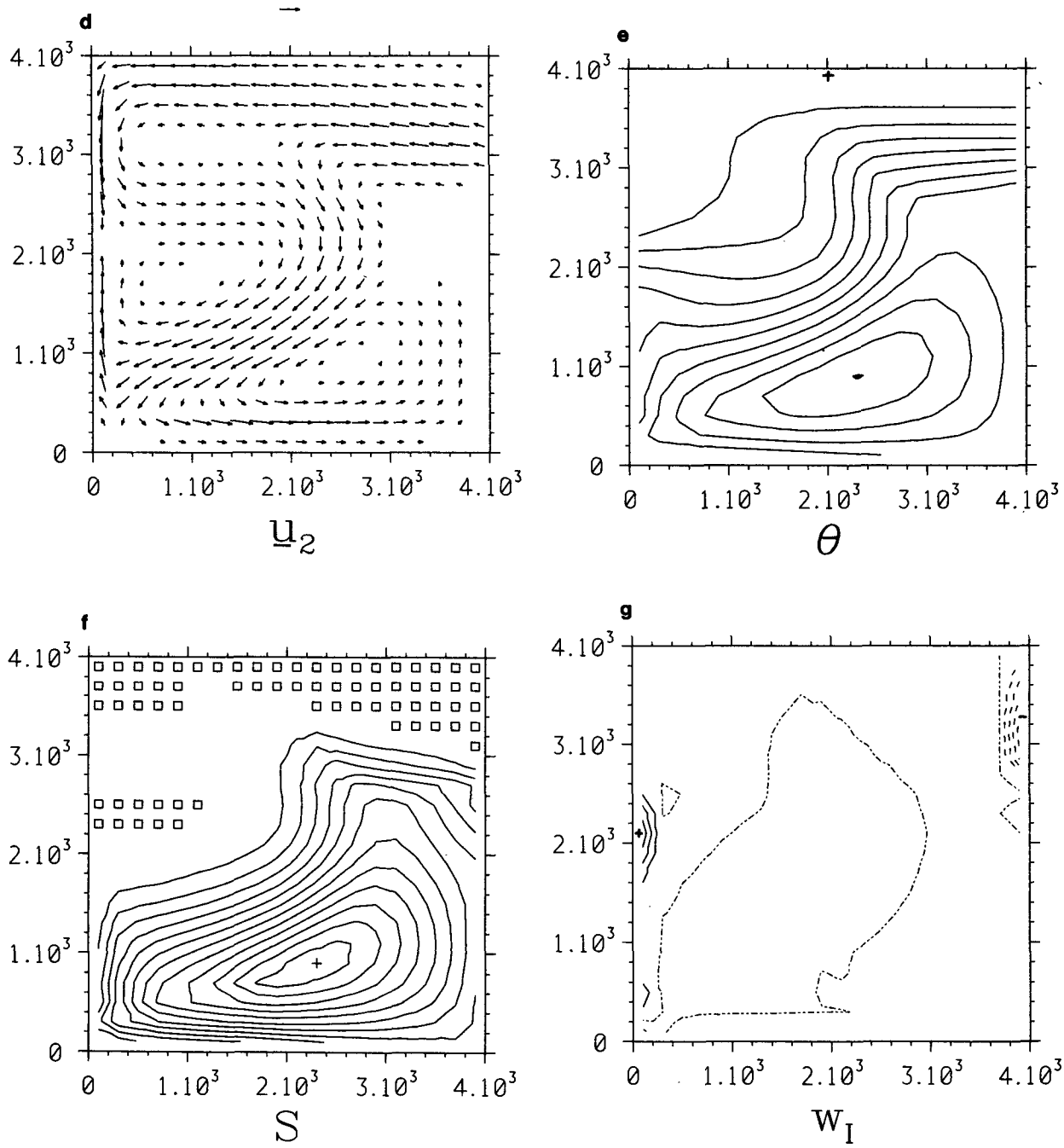

FIG. 6. (*Continued*)

where ϕ represents a possible convective effect. Integrating (6.1) over the entire basin, and use of the boundary conditions, yields

$$\int w_s\bar{\rho}_s dxdy = \int \phi dxdy = \int_{w_s>0} w_s\rho_1 dxdy + \int_{w_s<0} w_s\rho_s dxdy. \quad (6.2)$$

Assuming (as used here) that w_s and ρ_s are antisymmetric about $y = M/2$, (6.2) becomes

$$\int \phi dxdy = \int dx \int_0^{M/2} |w_s(y)|(\rho_1(M-y) - \rho_s(y))dy. \quad (6.3)$$

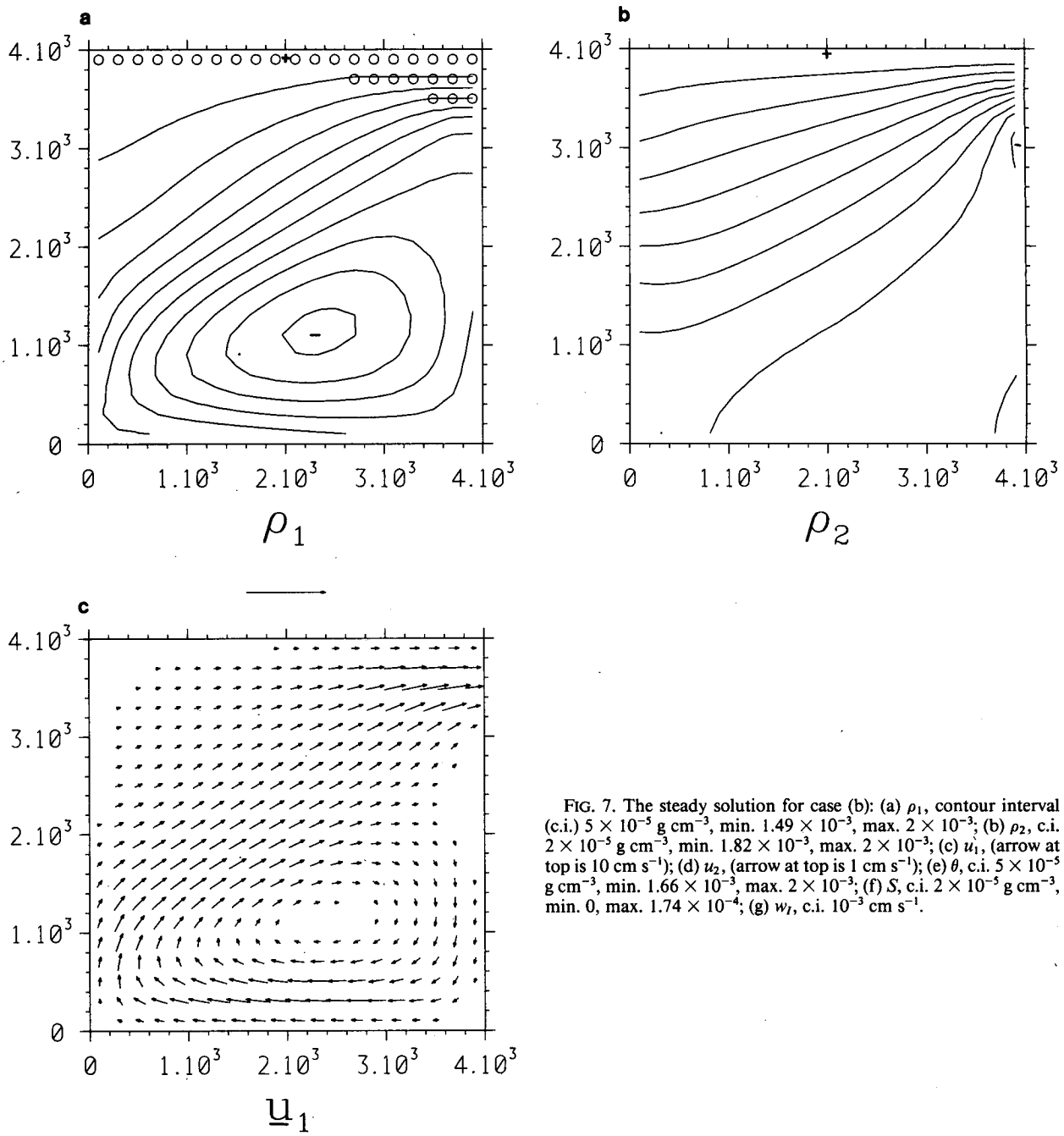

FIG. 7. The steady solution for case (b): (a) ρ_1, contour interval (c.i.) 5×10^{-5} g cm^{-3}, min. 1.49×10^{-3}, max. 2×10^{-3}; (b) ρ_2, c.i. 2×10^{-5} g cm^{-3}, min. 1.82×10^{-3}, max. 2×10^{-3}; (c) u_1, (arrow at top is 10 cm s^{-1}); (d) u_2, (arrow at top is 1 cm s^{-1}); (e) θ, c.i. 5×10^{-5} g cm^{-3}, min. 1.66×10^{-3}, max. 2×10^{-3}; (f) S, c.i. 2×10^{-5} g cm^{-3}, min. 0, max. 1.74×10^{-4}; (g) w_I, c.i. 10^{-3} cm s^{-1}.

Now $\rho_1(M - y) \geq \rho_s(M - y)$, or else the fluid would be unstably stratified, so that

$$\rho_1(M - y) - \rho_s(y) \geq \rho_s(M - y) - \rho_s(y) > 0.$$

Hence,

$$\int \phi dxdy > 0 \qquad (6.4)$$

so that overturning must occur either from the Ekman layer to level 1 or between levels 1 and 2.

Separate, and general, arguments now prove that convection occurs both between levels and from Ekman layer to level 1. In the lower level, ρ_2 must reach a maximal extremum somewhere—(x_0, y_0), say. If this is in the interior, this will be a local maximum; if at the boundary, its normal derivative vanishes by the

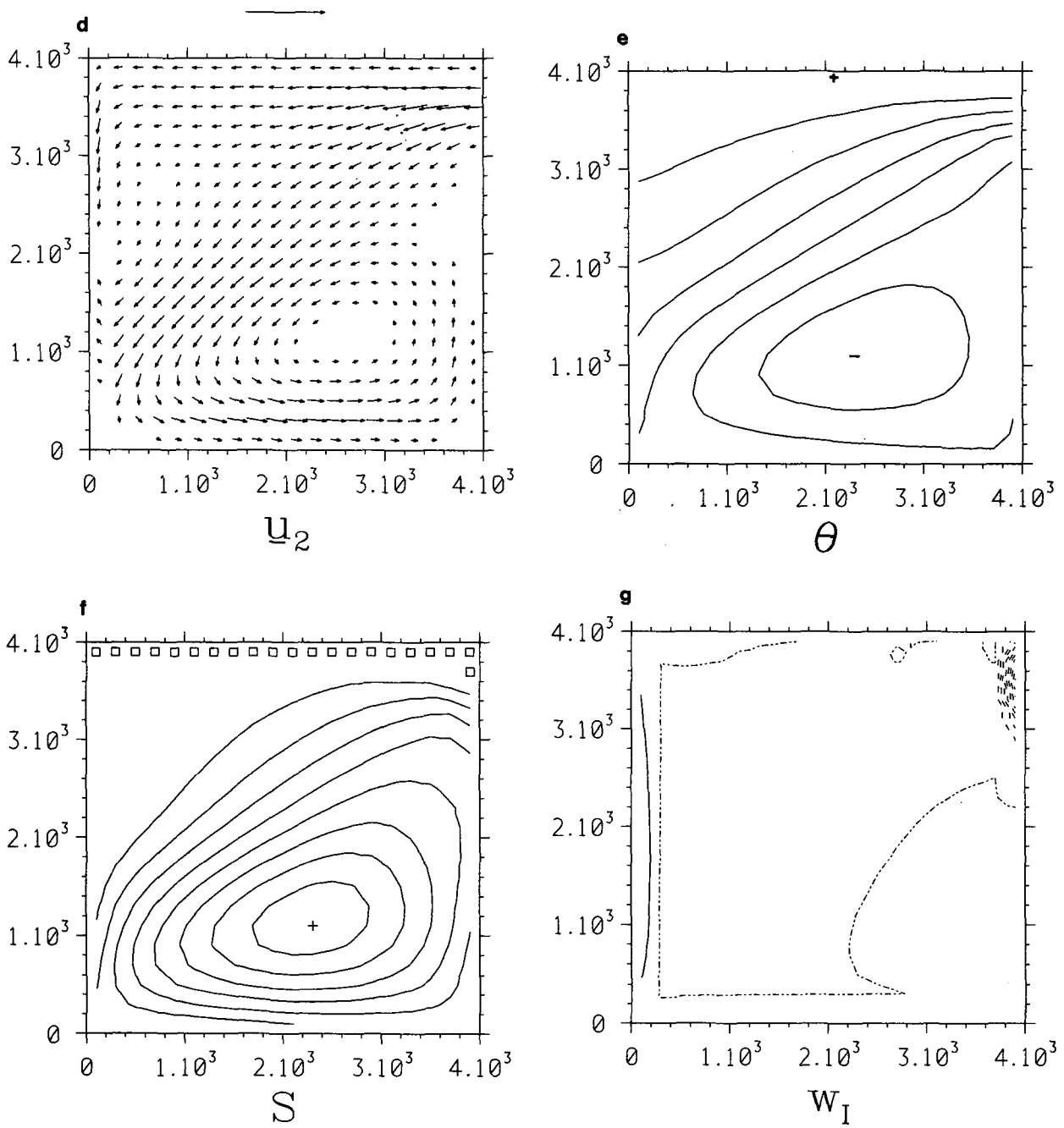

FIG. 7. (*Continued*)

boundary condition. In both cases, at (x_0, y_0) the steady version of (2.4) gives

$$\nabla \cdot (\mathbf{u}_2 \rho_2) + \frac{w_I \bar{\rho}_I}{H_2} = D_2 + \phi_2, \quad \mathbf{x} = \mathbf{x}_0 \qquad (6.5)$$

where $D_2 < 0$ represents diffusion and ϕ_2 the possible overturning. Rewriting the first term, using $\nabla \rho_2 = 0$ and (2.2), we have

$$\frac{w_I}{H_2}(\bar{\rho}_I - \rho_2) = D_2 + \phi_2, \quad \mathbf{x} = \mathbf{x}_0. \qquad (6.6)$$

Now, (2.6) implies that (i) if $w_I > 0$, $\bar{\rho}_I = \rho_2$ and so $\phi_2 > 0$; and (ii) if $w_I < 0$, $\bar{\rho}_I = \rho_1 \leqslant \rho_2$ and so $\phi_2 > 0$ again. In both cases, therefore,

$$\phi_2 > 0, \quad \mathbf{x} = \mathbf{x}_0 \qquad (6.7)$$

and so there is active convection where ρ_2 is maximal, extending to the bottom. As a corollary, $\rho_1 = \rho_2$, $\nabla\rho_1 = \nabla\rho_2 = 0$ at (x_0, y_0).

We now expand (6.1) in a similar manner:

$$H_1\rho_1\nabla\cdot\mathbf{u}_1 + H_2\rho_2\nabla\cdot\mathbf{u}_2 + w_s\bar{\rho}_s = D + H_1\phi_s + H_1\phi_1 + H_2\phi_2, \quad \mathbf{x} = \mathbf{x}_0 \tag{6.8}$$

where $D < 0$ is the depth integrated diffusion, ϕ_s is the possible surface to level 1 overturning, and ϕ_i the level 1 to 2 overturning effect at level i. We note that

$$H_1\phi_1 + H_2\phi_2 = 0 \tag{6.9}$$

for a steady state. Using (2.1), (2.2), and the equality of densities, (6.8) becomes

$$w_s(\bar{\rho}_s - \rho_1) = D + H_1\phi_s, \quad \mathbf{x} = \mathbf{x}_0. \tag{6.10}$$

If (i) $w_s > 0$, $\bar{\rho}_s = \rho_1$ and $\phi_s > 0$; while if (ii) $w_s < 0$, $\bar{\rho}_s = \rho_s$ and $\bar{\rho}_s \leqslant \rho_1$ so $\phi_s > 0$ again. Hence,

$$\phi_s > 0, \quad \mathbf{x} = \mathbf{x}_0 \tag{6.11}$$

so that overturning occurs from the Ekman layer into the top level, and, by (6.7), the bottom level as well.

Since ρ_1, ρ_2 cannot exceed the maximum value of ρ_s, convection must occur in the region of this maximum (along the northern boundary in the cases studied here). The extent of this region, and the possible occurrence of other areas of overturning, are difficult nonlinear problems and will not be addressed here.

Overturning causes problems with eastern boundary conditions. The condition $u = 0$ is applied on $x = L$, yet $\theta_y = \rho_{sy}$ in a region of overturn, and $\hat{u}$ varies as θ_y. A discontinuity is thus produced near the boundary: one of many possible connected with the still unsolved problem of relevant boundary conditions for the thermocline equations (Huang, 1984).

b. *Scaling arguments*

Scaling arguments may be examined to show that certain terms may be neglected and to deduce some qualitative features about the solution. There are two relevant scalings depending on the importance of diffusion; we examine the more relevant case of advection dominating diffusion (as measured by a Peclet number, $w_{so}L^2/H_1\kappa_T$, being large).

Let us first discuss how large $\hat{\mathbf{u}}$ (or equivalently, $\Delta\theta$, a measure of the variation of θ) ought to be. If $\Delta\theta$ were as large as $\Delta\rho_s$ (a measure of the variation in ρ_s), an estimate from (3.13) would be

$$\hat{u}_\theta = \frac{gH\Delta\theta}{\rho_0 f_0 L} = \frac{gH\Delta\rho_s}{\rho_0 f_0 L}. \tag{6.12}$$

Another estimate would be to require from mass conservation

$$\hat{u}_w = \frac{Lw_{so}}{H_1}. \tag{6.13}$$

These two estimates are not the same in general. In fact,

$$\left(\frac{\hat{u}_w}{\hat{u}_\theta}\right)^{1/2} = \left(\frac{\rho_0 f_0 L^2 w_{so}}{gH_1 H\Delta\rho_s}\right)^{1/2} = \mu. \tag{6.14}$$

Here the small quantity μ takes the values 0.15 and 0.05 as $w_{so} = 10^{-4}$, 10^{-5} cm s^{-1}. To accommodate this difference, $\Delta\theta$ must become

$$\Delta\theta = \mu\Delta\rho_s \tag{6.15}$$

equaling 6×10^{-4}, 2×10^{-4} gm cm^{-3} as $w_{so} = 10^{-4}$, 10^{-5} cm s^{-1}. Thus, a scale for $\hat{u}$ is

$$\hat{u} = (\hat{u}_w\hat{u}_\theta)^{1/2} = \left(\frac{gHw_{so}\Delta\rho_s}{\rho_0 f_0 H_1}\right)^{1/2} \tag{6.16}$$

which equals 6.5, 2 cm s^{-1} as $w_{so} = 10^{-4}$, 10^{-5} cm s^{-1}. These estimates are in excellent agreement with the computed solutions, and are similar to those made by Welander (1971) for the continuous problem.

Now S vanishes in regions of overturning, and is positive elsewhere; hence, S scales on $\mu\Delta\rho_s$. However, θ is constrained to equal ρ_s in regions of overturning, so that the magnitude of θ is $\Delta\rho_s$, although its variation is typically $O(\mu)$ smaller, by (6.15). This suggests that the area of overturning must also vary as some power of μ (depending on the spatial structure of ρ_s near the northern boundary) to maintain the variation in θ in (6.15). Thus, *the area of the overturning increases both with the strength of the wind-driven circulation and with the buoyancy variation.*

This yields approximate scalings for the variables as:

$$\begin{aligned} U, V, Q \quad &\text{on} \quad \frac{f_0 w_{so}}{\beta H}; \\ \hat{u}, \hat{v} \quad &\text{on} \quad \mu\frac{gH\Delta\rho_s}{\rho_0 f_0 L}; \\ \Delta\theta, S, \Delta\rho_1, \Delta\rho_2 \quad &\text{on} \quad \mu\Delta\rho_s; \\ x, y \quad &\text{on} \quad L. \end{aligned} \tag{6.17}$$

Rewriting the steady versions of (2.3) and (2.4) and ignoring overturning, gives

$$(1-\delta)\hat{\mathbf{u}}\cdot\nabla(\theta - S) + \mathbf{U}\cdot\nabla(\theta - S) + 2S\frac{(1-\delta)}{\delta}\nabla\cdot(\mathbf{U} - \delta\hat{\mathbf{u}})\bar{H}[-\nabla\cdot(\mathbf{U} - \delta\hat{\mathbf{u}})] + \frac{w_s}{H_1}(\rho_s - \theta + S)\bar{H}(-w_s) = \kappa_T\nabla^2(\theta - S) \tag{6.18}$$

$$-\delta\hat{\mathbf{u}}\cdot\nabla(\theta + S) + \mathbf{U}\cdot\nabla(\theta + S) + 2S\nabla\cdot(\mathbf{U} - \delta\hat{\mathbf{u}})\bar{H}[\nabla\cdot(\mathbf{U} - \delta\hat{\mathbf{u}})] = \kappa_T\nabla^2(\theta + S) \tag{6.19}$$

where

$$\delta = H_1/H \tag{6.20}$$

is a depth ratio. Actually it is unnecessary to nondimensionalize since analytic solutions cannot be found.

Instead, we simply compare terms. Note that $\nabla \cdot \hat{\mathbf{u}} \ll \hat{u}_x$ by (3.15), but $\delta \nabla \cdot \hat{\mathbf{u}}$ is still about 3 (9) times larger than $\nabla \cdot \mathbf{U}$ according as $w_{so} = 10^{-4}$, 10^{-5} cm s^{-1}. After evaluation and comparison of terms, (6.18) and (6.19) reduce approximately to

$$-(1-\delta)\hat{\mathbf{u}} \cdot \nabla S - 2(1-\delta) S \nabla \cdot \hat{\mathbf{u}} \bar{H}(\nabla \cdot \hat{\mathbf{u}}) + \frac{w_s}{H_1}(\rho_s - \theta)\bar{H}(-w_s) = 0 \quad (6.21)$$

$$-\delta \hat{\mathbf{u}} \cdot \nabla S + \mathbf{U} \cdot \nabla(\theta + S) - 2\delta S \nabla \cdot \hat{\mathbf{u}} \bar{H}(-\nabla \cdot \hat{\mathbf{u}}) = 0. \quad (6.22)$$

(Note that $\nabla \cdot \mathbf{U}$ has been neglected against $\delta \nabla \cdot \hat{\mathbf{u}}$ for simplicity.) Diffusion does not appear in these approximate balances except where w_s becomes small, and the barotropic flow appears only in the lower level.

These equations remain complicated, mostly because of the one-sided differences, and no combinations of them yield any simplifications. However, we may isolate four distinct regimes depending on the signs of w_s and $\nabla \cdot \hat{\mathbf{u}}$. Of these, only those for which the $\nabla \cdot \hat{\mathbf{u}}$ terms vanish in (6.21) are of interest. If $\nabla \cdot \hat{\mathbf{u}}$ is negative (i.e., $\hat{v} > 0$), (6.21) becomes

$$\hat{\mathbf{u}} \cdot \nabla S = \frac{w_s}{(1-\delta)H_1}(\rho_s - \theta)\bar{H}(-w_s) \quad (6.23)$$

and the rhs in the northern basin vanishes. Then, S is advected by the $\hat{\mathbf{u}}$ field, or, equivalently, S is a function of θ. This is clearly seen in Figs. 6e and 6f in the northward flowing jet, for example, where S and θ contours are exactly overlaid. In such a region we may also examine (6.22), which becomes

$$\delta \hat{\mathbf{u}} \cdot \nabla S = \mathbf{U} \cdot \nabla \rho_2 - 2\delta S \nabla \cdot \hat{\mathbf{u}} \quad (6.24)$$

i.e.,

$$\mathbf{U} \cdot \nabla \rho_2 < 0 \quad (6.25)$$

so that the lower level density decreases eastwards as it is advected across the northward jet, again as observed.

If w_s is negative but $\nabla \cdot \hat{\mathbf{u}}$ remains negative, the region of applicability is the northwestern half of the southern gyre. Here, (6.23) implies

$$\hat{\mathbf{u}} \cdot \nabla S > 0 \quad (6.26)$$

so that streamlines for the upper level flow (roughly $\hat{\mathbf{u}}$) must cross S contours so as to increase S in the direction of flow. Comparison of Figs. 6c and 6f confirms this feature.

Although useful, these results underline the intrinsically nonlinear character of the thermocline equations; even this simple model is analytically intractable.

c. *Initial spinup*

We examine the process when Ekman pumping and buoyancy are turned on from rest. Linearizing the response about the initial stratification $\bar{\rho}_1$, $\bar{\rho}_2$, (2.3) and (2.4) become, neglecting overturn,

$$\rho_{1t} + (\bar{\rho}_1 - \bar{\rho}_I)\nabla \cdot \mathbf{u}_1 = -\frac{w_s}{H_1}(\bar{\rho}_s - \bar{\rho}_I)$$

$$\rho_{2t} + (\bar{\rho}_2 - \bar{\rho}_I)\nabla \cdot \mathbf{u}_2 = 0. \quad (6.27)$$

After adding, and a little algebra, this yields

$$2\theta_t + \frac{gH}{2f_0^2\rho_0}[(1-\delta)(\bar{\rho}_1 - \bar{\rho}_I) - \delta(\bar{\rho}_2 - \bar{\rho}_I)](\beta\theta_x + \kappa\theta_{xx}) = \frac{w_s}{H_1}(\bar{\rho}_I - \bar{\rho}_s) \quad (6.28)$$

which takes the form of a long Rossby wave equation, damped slightly by the terms of order κ. Initially, w_I is dominated by w_s so that in the subtropics the undamped wave satisfies

$$\theta_t - \frac{\beta g H_1 \bar{S}}{2f^2\rho_0}\theta_x = \frac{w_s}{2H_1}(\bar{\rho}_1 - \rho_s). \quad (6.29)$$

This travels westward at speed $\beta g H_1 \bar{S}/2f^2\rho_0$ leaving the Sverdrup solution

$$\theta_x = -\frac{w_s(\bar{\rho}_1 - \rho_s)f^2\rho_0}{2\beta g H_1^2 \bar{S}} \quad (6.30)$$

behind it. It is straightforward to show that this does not initially alter the sign of w_I. In the subpolar region, w_s is positive and θ satisfies

$$\theta_t - \frac{\beta g H_2 \bar{S}}{2f^2\rho_0}\theta_x = \frac{w_s \bar{S}}{H_1} \quad (6.31)$$

whose speed is formally faster, despite the increase in f.

A qualitative picture of the spinup process now emerges. At time zero, θ is constant, and the forcing (which is independent of x) begins to spin up the entire basin linearly in time. Information about the eastern boundary, where the requirement of no normal flow means that θ_y approximately vanishes by (3.14), propagates westwards, leaving an essentially steady Sverdrup-like solution behind it. The process is identical to the insulated wind-driven problem of Anderson and Gill (1975) where windstress is inserted into a vertical normal mode. In that case, the forcing in the θ equation is replaced by $(\bar{\rho}fH_1)^{-1}\bar{S}\,\mathrm{curl}\tau$, for some windstress τ. From the definition of w_s, this is formally of the same order as the forcing in (6.29), although the baroclinic velocity response would be more rapid because of the direct wind forcing.

These arguments establish the two wavelike timescales. The shorter is the long Rossby wave transit time

$$\frac{2f^2\rho_0 L}{\beta g H_1 \bar{S}}$$

of order a few years, depending on the initial stratification, and the longer is the spindown time for the damped Rossby wave for the linear drag κ,

$$\frac{2f^2\rho_0 L^2}{\kappa g H \bar{S}}$$

of order a century for the values used here. The largest timescale is the diffusive scale L^2/κ_T, as mentioned previously.

d. Transfer between gyres

In either the layer model of Luyten *et al.* (1983), or in a continuously stratified fluid, it may be shown that there is no flow across the latitude where w_s vanishes (e.g., Huang, 1984), except in the western boundary layer. In the current level model, a strong flow is observed between the gyres ($y = M/2$) in the interior (Fig. 6c). What is the origin of this flow?

Taking $(1 - \delta)^{-1}$ times (2.3) plus δ^{-1} times (2.4) at $y = M/2$ (where $V = w_s = 0$) gives

$$2\hat{\mathbf{u}} \cdot \nabla\theta - \kappa_T\left(\frac{\nabla^2\rho_1}{(1-\delta)} - \frac{\nabla^2\rho_2}{\delta}\right) = \frac{2Sw_I H}{H_1 H_2}[\bar{H}(w_I) - \bar{H}(-w_I)], \quad y = M/2. \quad (6.32)$$

If κ_T and κ are both negligible, the lhs vanishes, implying that w_I vanishes, and hence $\hat{v}$ also, giving no gyre transfer. Since estimates of (6.32) show both effects to be important, *transfer between gyres is driven both by diffusion and by ageostrophic effects.* As a check, a calculation with κ_T halved yielded a narrower region of northward flow between the gyres.

7. Particle trajectories

The solutions of the previous sections were quite complicated, although the resulting flow fields were well behaved. Nonetheless, such solutions conceal many features of interest, in particular the ventilation of the subtropical gyre. This topic is discussed by Luyten *et al.* (1983), who conclude that for their multislab model of a northern basin, a considerable portion of the deep subtropics consists of water which has never been in contact with the surface.

Rhines and Young (1982) were also concerned with the depth to which surface effects could reach. They concluded, on the basis of closed potential vorticity contours, that a suitable scale was

$$D = \frac{f}{N}(U/\beta)^{1/2}, \quad (7.1)$$

where N is the buoyancy frequency and U is a velocity scale. The same scale emerges from the differential equations for the thermocline problem (Killworth, 1983a) and can be thought of as the vertical scale associated with quasigeostrophic motions with a horizontal scale equal to the Rhines scale $(U/\beta)^{1/2}$.

In the level model, the depths to which water particles sink depend on the signs and sizes of w_s and w_I. The sign of w_s is specified, and we can obtain w_I either from Fig. 6g directly or from

$$w_I = (1 - \delta)\left(w_s - \frac{\beta H_1}{f}\hat{v}\right) \quad (7.2)$$

from the definitions in Section 2. Using the scalings in Section 6, $\beta H_1\hat{v}/fw_s \approx 5$ for case (a), so that w_I varies roughly as $-\hat{v}$. Since $\mathbf{u}_1$ and $\hat{\mathbf{u}}$ are fairly similar, Fig. 6c shows that w_I can take either sign in either basin. It is thus impossible to define a depth of sinking for water particles, since in the several years it takes a particle to descend 400 m (H_1) at a speed of several times 10^{-4} cm s^{-1}, the particle will pass completely around a gyre and pass through regions of positive and negative w_I. So the only way to investigate particle motions is to follow particles directly.

Nonetheless, we may still estimate (7.1) using the scalings of Section 6. We use $N^2 \approx gS/\rho_0 H_1$ to find

$$D \approx \left(\frac{fH_1 H}{\beta L}\right)^{1/2} \approx \epsilon^{-1/2}(H_1 H)^{1/2} \approx 1.5 \text{ km} \quad (7.3)$$

which, surprisingly, is only a geometric result and does not depend on the magnitude of either forcing (note that a measure of stratification is assumed in the choice of H_1).

To understand the ventilation of the lower subtropical level, we return to the problem of particle trajectories. For the simple dynamics in this paper, it involves solving for particle position (X, Y, Z) from

$$\frac{dX}{dt} = u_i(X, Y) \quad (7.4)$$

$$\frac{dY}{dt} = v_i(X, Y) \quad (7.5)$$

$$\frac{dZ}{dt} = \tilde{w}(X, Y) \quad (7.6)$$

$$i = 1, \quad Z > -H_1; \quad i = 2, \quad Z < -H_1 \quad (7.7)$$

and $\tilde{w}$ is the linear interpolation of either w_s and w_I (level 1) or w_I and 0 (level 2).

Particles are assumed to leave the base of the Ekman layer in the subtropical gyre, where w_s is downwards, and then follow (7.4)–(7.7). As examples of the very different behavior which can ensue, consider Figs. 8–11, which show particles injected at 700 km north, with X values of 500, 1300, 2100, and 2900 km east of the western boundary.

Figure 8 shows the 500 km particle. This lies on the separated current which flows northeast across the basin, and follows this current, gradually descending, for a year before being deposited in the slower region near

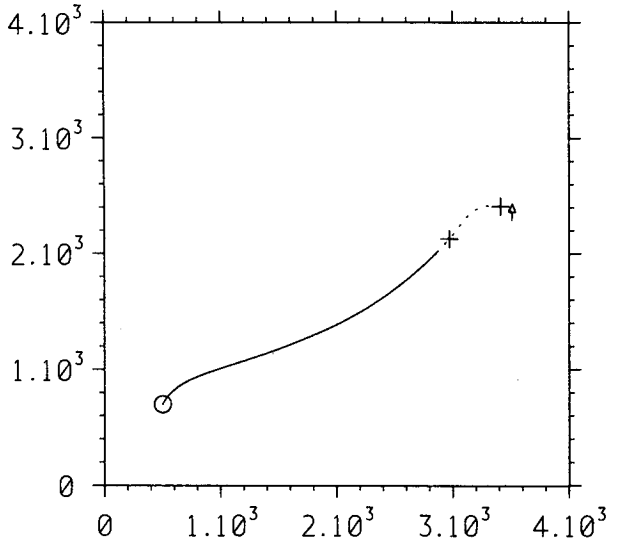

FIG. 8. Particle trajectory for case (a), $X = 500$ km, $Y = 700$ km. Circle marks injection point from Ekman layer. Solid line denotes downward movement; dashed line upward movement. Crosses drawn every year. An arrow marks the point of upwelling into the subpolar Ekman layer.

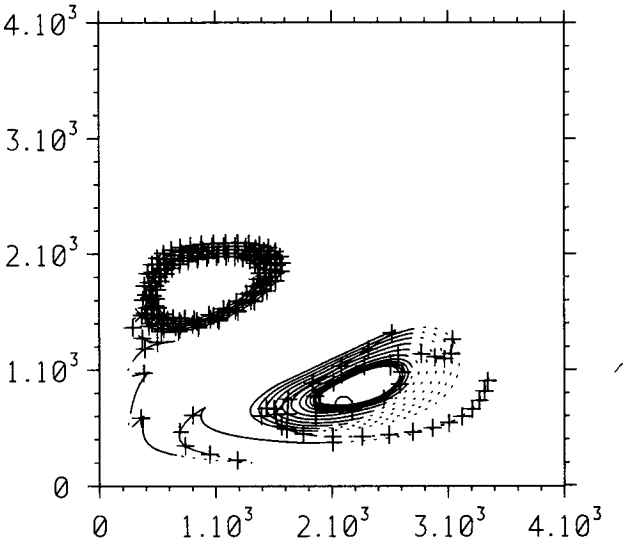

FIG. 10. As in Fig. 8 but for $X = 2100$ km.

the eastern boundary, where it upwells and reaches the surface. Figure 9 shows the 1300 km particle, whose path is much more complex. It spends many years in the anticyclonic southern gyre, rising in the east and sinking in the west, and gradually diverging outwards. It then passes into the subpolar region, and reaches a near stagnation point near the eastern boundary. Here, it drops to the lower level after many years, and slowly retraces its path, now at depth, into the southern gyre which it now follows cyclonically. It suffers several reversals of direction, caused by transition between levels, and its track has not terminated in the figure. Thus, this particle ventilates the deep subtropics only via the deep subpolar region.

The 2100 km particle is shown in Fig. 10. After some years in the subtropical gyre, it descends to the lower level and diverges slowly outward. It rises in the east and moves rapidly west, then executes a jagged motion, caused again by transition between levels, and finally ends up in the weak deep descending gyre shown in Fig. 6d. Finally, the 2900 km particle (Fig. 11) also

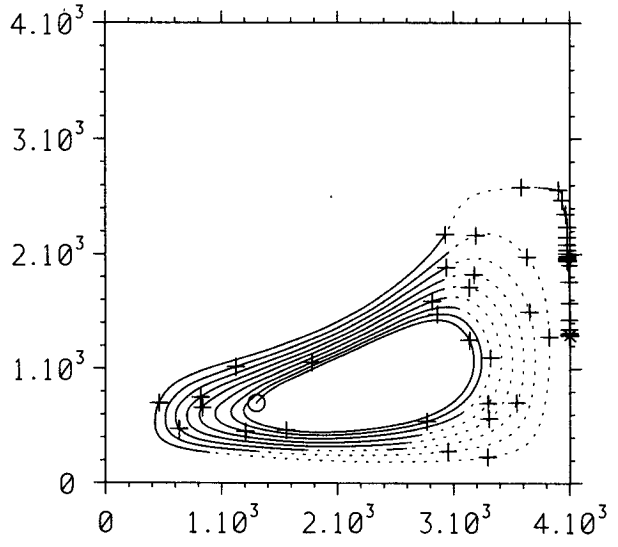

FIG. 9. As in Fig. 8 but for $X = 1300$ km.

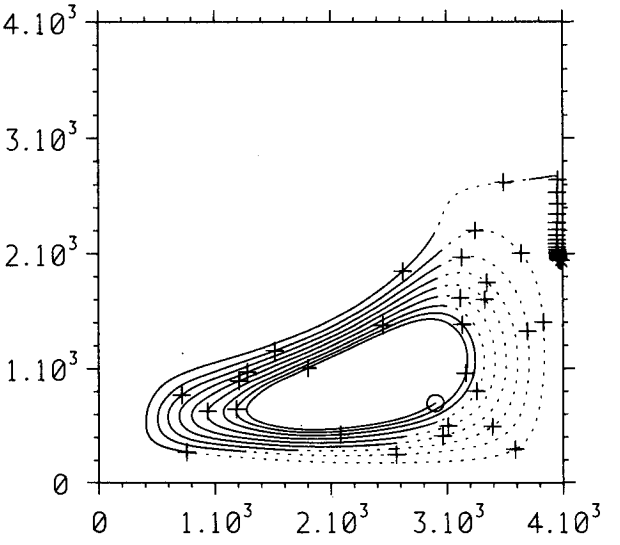

FIG. 11. As in Fig. 8 but for $X = 2900$ km.

spirals slowly out, reaches the subpolar region near the east wall, and propagates slowly south over many years.

These particles are chosen from calculations repeated every 400 km across the basin, but their range of behaviour typifies all the responses. Only on rare occasional does a particle reach the deep subtropics by direct sinking.

The calculations were repeated with particles beginning at 1700 km north, just south of the zero wind stress curl line, and perhaps rather more relevant to the Luyten *et al.* (1983) calculation. Particles originating at X values less than 2500 km moved north a few hundred km and surfaced. Those 2900 km or more from the western boundary (i.e., 1100 km or closer to the eastern boundary) produced tracks similar to the 2900 km particle in Fig. 11. These latter superficially resemble the Luyten *et al.* (1983) solution, except that there is both up- and downwelling, where their solution would imply only downwelling.

Particle motions in a diffusive fluid are not well described by a purely advective model. In order to simulate the effects of the (small) diffusion in the model, the particle trajectories were repeated but this time for an ensemble of particles all originating at the same point. At each time step, each particle was advected by (7.4)–(7.7), and then moved in a random horizontal direction a distance $(\kappa_T \Delta t)^{1/2}$, where Δt is the time step used in the simulation.

Figure 12 shows a typical example for particles originating at X = 2900 km. The general picture remains qualitatively similar to those without diffusion, but notice how very scattered are the endpoints of the calculation. Particles either remain within the anticyclonic subtropical gyre, or are ejected from it into the northern basin where the motion is less well organized.

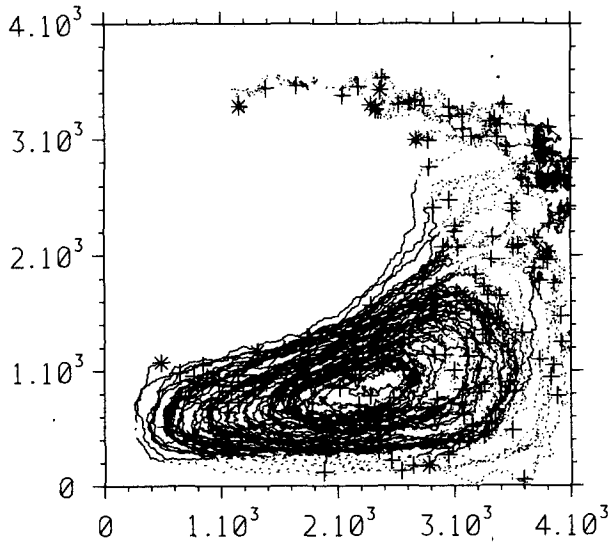

FIG. 12. As in Fig. 11 but for an ensemble of ten particles for 20 years, and a random walk as described in the text. The end of each track is shown by an asterisk.

Thus, little of the deep subtropical gyre seems to be ventilated. The western area, which is partially ventilated, achieves this by a complex series of flow interactions between subpolar and subtropical gyres, in a manner which is presumably highly model dependent (e.g., Young, 1984).

8. Discussion

This paper has described a simple numerical model that attempts to reproduce the thermocline dynamics. Unlike the multislab model of Luyten *et al.* (1983), which could not permit realistic horizontal stratification but allowed in principle a well resolved vertical structure, the use of a two-level model permits realistic horizontal stratification but very poor vertical resolution.

Even given such simple dynamics, the resulting solutions are quite complicated, with convective overturning a key ingredient in the production of a steady state solution. Within the limited model framework, the solutions are fairly realistic.

The model here "finesses" certain fundamental problems related to thermocline dynamics, specifically the sidewall boundary conditions. For zero diffusion, it is possible to show that for a continuously stratified model, a plane eastern boundary must possess uniform density (Killworth, 1983b; Huang, 1984). In the slab models, this appears as a requirement of vanishing layer depth for all but one of the layers, whose depth is uniform (no matter how many layers). In the level model here, θ is essentially uniform on the eastern boundary but S varies. If the number of levels were increased, all the interface mean densities would become uniform along the boundary, with one measure of stratification still able to vary. Neither model is thus a satisfactory reproduction of reality (which has a strong northward density gradient at the east coast). Pedlosky (1983a) circumvents the problem by permitting an unspecified flow connection between the various layers of the slab model, but one probably needs a more complete eastern boundary layer specification to proceed further.

It would be interesting to employ various closure schemes for the western boundary layer, rather than the simple Stommel formulation used here. The potential vorticity and buoyancy distributions in the interior surely depend strongly on the degree and form of mixing in this layer (cf. Young, 1984), and the solution in this simple model may be dependent on these details. Further discussion must await future papers.

Several extensions to this model could be made. It is straightforward to add more levels to produce fluid remote from both surface forcing and the rigid bottom. However, a more realistic model that still retained the thermocline physics, and one which would allow more freedom in the surface forcing, would be to make the Ekman layer into an active dynamical level. In such a model, wind stress would be inserted into the new sur-

face level exactly as in the Bryan (1969) model. The dynamics of this level would be geostrophy plus wind stress. There would be a buoyancy forcing at the surface, perhaps a Haney (1971) relaxation to atmospheric value. Such a model would allow a more complete investigation of the coupling between wind and buoyancy forcing than the current model permits, and it is hoped to report on this model at a later date.

Acknowledgments. This work was supported by a grant from the EEC. The programming was ably undertaken by J. R. Blundell, who also provided useful comments on the manuscript. Suggestions by a referee of an early version of this paper, and by F. Bretherton, were most useful.

APPENDIX

The Numerical Boundary Instability

Consider the flow near the western boundary as in Fig. 13 and linearization about some mean stratification $\bar{\rho}_1, \bar{\rho}_2$. The buoyancy conservation equations, neglecting diffusion and forcing, become

$$\frac{\partial \rho_1}{\partial t} + \bar{\rho}_1 \nabla \cdot \mathbf{u}_1 - \frac{w_I \bar{\rho}_I}{H_1} = 0 \tag{A1}$$

$$\frac{\partial \rho_2}{\partial t} + \bar{\rho}_2 \nabla \cdot \mathbf{u}_2 + \frac{w_I \bar{\rho}_I}{H_2} = 0; \tag{A2}$$

i.e.,

$$\frac{\partial \rho_1}{\partial t} + (\bar{\rho}_1 - \bar{\rho}_I) \nabla \cdot \mathbf{u}_1 = 0 \tag{A3}$$

$$\frac{\partial \rho_2}{\partial t} + (\bar{\rho}_2 - \bar{\rho}_I) \nabla \cdot \mathbf{u}_2 = 0. \tag{A4}$$

Using the definition of $\bar{\rho}_I$ and adding gives

$$\frac{\partial \theta}{\partial t} = \bar{S}(\nabla \cdot \mathbf{U} + (1 - \delta) \nabla \cdot \hat{\mathbf{u}}) \tag{A5}$$

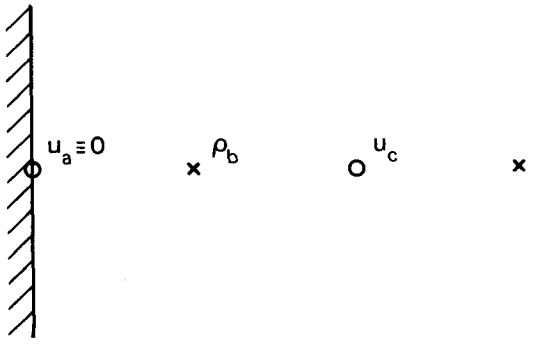

FIG. 13. Notation for the Appendix.

in upwelling regions and

$$\frac{\partial \theta}{\partial t} = \bar{S}(-\nabla \cdot \mathbf{U} + \delta \nabla \cdot \hat{\mathbf{u}}) \tag{A6}$$

in downwelling regions. In either case, the first term is a known constant forcing. The second term is proportional to $\nabla \cdot \hat{\mathbf{u}}$. (Such a term also occurs with centered differences.) We evaluate $\nabla \cdot \hat{\mathbf{u}}$ at the point b in Fig. 13 and it has two components. The first is

$$\hat{u}_x = \frac{\hat{u}_c - 0}{\Delta x} = \frac{\hat{u}_c}{\Delta x} \tag{A7}$$

and the second is $\hat{v}_y$. Except near the boundary $\hat{v}_y$ will be of the same order as $\hat{u}_x$, but at the first grid point the divergence is dominated by the sudden change from geostrophy (at c) to zero normal velocity (at a). Thus,

$$\frac{\partial \theta_b}{\partial t} \approx \frac{\alpha \bar{S}}{\Delta x} \hat{u}_c \tag{A8}$$

$$\approx \frac{\alpha \bar{S} g H}{2 f \rho_0 \Delta x} \theta_y \tag{A9}$$

by (3.14), neglecting the viscous term, where α is either $(1 - \delta)$ or δ.

The form of (A9) is thus a wave equation along the boundary, whose speed C is given by $c^2/f\Delta x$, where c is the speed of the first baroclinic internal wave mode, here equal to $(\alpha g H \bar{S}/2\rho_0)^{1/2}$. This result immediately generalizes to a multilevel model.

The *CFL* criterion must therefore be satisfied for (A9), despite the fact that the wave is of numerical and not physical origin. Thus,

$$\frac{C\Delta t}{\Delta y} = \frac{c^2 \Delta t}{f \Delta x \Delta y} = \frac{\alpha g H \bar{S} \Delta t}{2\rho_0 f \Delta x \Delta y} < 1 \tag{A10}$$

together with a rather stronger condition in the corners of the domain where waves in both horizontal directions come into play.

Since C varies inversely as Δx or Δy, the finer the resolution the more restrictive is the choice of time step. The restrictions also grow nearer the equator, where f is smaller. With our choice of 200 km grid spacing, a time step of 1 day is just stable. It is possible to use the definitions of $\mathbf{u}_1$, $\mathbf{u}_2$ to eliminate this numerical mode. The increase in time step allowed is not worth the added complexity in boundary conditions for this simple model, but might be so in multilayered models.

REFERENCES

Anderson, D. L. T., and A. E. Gill, 1975: Spin-up of a stratified ocean with applications to upwelling. *Deep-Sea Res.*, **22**, 583–596.

Bryan, K., 1969: A numerical method for the study of the circulation of the world ocean. *J. Comput. Phys.*, **4**, 347–376.

Cox, M. D., and K. Bryan, 1984: A numerical model of the ventilated thermocline. *J. Phys. Oceanogr.*, **14**, 674–687.

Davey, M. K., 1983: A two-level model of a thermally forced ocean basin. *J. Phys. Oceanogr.*, **13,** 169–190.

Esbensen, S. K., and Y. Kushnir, 1981: The heat budget of the global ocean: An atlas based on estimates from surface marine observations. Climatic Research Institute Rep. No. 79, Oregon State University, Corvallis, 204 pp.

Haney, R. L., 1971: Surface thermal boundary conditions for ocean circulation models. *J. Phys. Oceanogr.*, **1,** 241–248.

Hasselmann, K., 1982: An ocean model for climate variability studies. Progress in Oceanography, Vol. 11, Pergamon, 69–92.

Huang, R. X., 1984: The thermocline and current structure in subtropical/subpolar basins. Ph.D. thesis, Woods Hole Oceanographic Institution, 218 pp.

Killworth, P. D., 1974: A baroclinic model of motions on Antarctic continental shelves. *Deep-Sea Res.*, **21,** 815–837.

——, 1983a: Absolute velocity computations from single hydrographic sections. *Deep-Sea Res.*, **30,** 513–542.

——, 1983b: Some thoughts on the thermocline equations. Ocean Modelling, No. 48, (unpublished manuscript).

Leetmaa, A., and A. F. Bunker, 1978: Updated chart of the mean annual wind stress, convergences in the Ekman layer and Sverdrup transports in the North Atlantic. *J. Mar. Res.*, **36,** 311–322.

Levitus, S., 1982: *Climatological Atlas of the World Ocean.* NOAA Prof. Pap. 13, U.S. Govt. Printing Office, Washington DC, 173 pp.

Luyten, J. R., J. Pedlosky and H. M. Stommel, 1983: The ventilated thermocline. *J. Phys. Oceanogr.*, **13,** 292–309.

McDowell, S., P. B. Rhines and T. Keffer, 1982: North Atlantic potential vorticity and its relation to the general circulation. *J. Phys. Oceanogr.*, **12,** 1417–1436.

Pedlosky, J., 1983a: Eastern boundary ventilation and the structure of the thermocline. *J. Phys. Oceanogr.*, **13,** 2038–2044.

——, 1983b: On the relative importance of ventilation and mixing of potential vorticity. *J. Phys. Oceanogr.*, **13,** 2121–2122.

——, and W. R. Young, 1983: Ventilation, potential vorticity homogenisation and the structure of the ocean thermocline. *J. Phys. Oceanogr.*, **13,** 2020–2037.

Rhines, P. B., and W. R. Young, 1982: A theory of the wind-driven circulation I. Mid-ocean gyres. *J. Mar. Res.*, **40** (Suppl.), 559–596.

Robinson, M. K., R. A. Bauer and E. H. Schroeder, 1979: *Atlas of North Atlantic-Indian Ocean Monthly Mean Temperatures and Mean Salinities of the Surface Layer.* U.S. Naval Oceanographic Office Ref. Publ. 18, Washington, DC, 234 pp.

Schott, F., and H. M. Stommel, 1978: Beta spirals and absolute vorticities in different oceans. *Deep-Sea Res.*, **25,** 961–1010.

Stommel, H. M., 1948: The westward intensification of wind-driven ocean currents. *Trans. Amer. Geophys. Union,* **29,** 202–206.

Welander, P., 1971: Some exact solutions to the equations describing an ideal-fluid thermocline. *J. Mar. Res.*, **29,** 60–68.

Worthington, L. V., 1970: The Norwegian Sea as a mediterranean basin. *Deep-Sea Res.*, **17,** 77–84.

Wunsch, C., and B. Grant, 1982: Towards the general circulation of the North Atlantic Ocean. Progress in Oceanography, Vol. 11, Pergamon, 1–59.

Young, W. R., 1984: The role of western boundary layers in gyre-scale ocean mixing. *J. Phys. Oceanogr.*, **14,** 478–483.